High pressure X-ray diffraction study of $SrMnO_3$ perovskite*

LIU Ying-Xin(刘迎新)[1,2] QIN Shan(秦善)[2;1)] WU Xiang(巫翔)[2]
JIANG Jian-Zhong(蒋建中)[3] Kikegawa Takumi[4] SHI Guang-Hai(施光海)[1]

[1] State Key Laboratory of Geological Processes and Mineral Resources, China University of Geosciences, Beijing 100083, China
[2] Department of Geology and Key Laboratory of Orogenic Belts and Crustal Evolution of MOE, Peking University, Beijing 100871, China
[3] International Center for New-structured Materials (ICNSM), Zhejiang University and Laboratory of New-structured Materials, Department of Materials Science and Engineering, Zhejiang University, Hangzhou 310027, China
[4] Institute of Materials Structure Science, High Energy Accelerator Research Organization, Tsukuba 3050801, Japan

Abstract: Using a diamond anvil cell device and synchrotron radiation, the in-situ high-pressure structure of $SrMnO_3$ has been investigated. At pressure up to 28.6 GPa, no pressure-induced phase transition is observed. The lattice parameters as a function of pressure is reported, and the relationship of the axial compression coefficients is $\beta_a > \beta_c$. The isothermal bulk modulus K_{298}=266(4) GPa is also obtained by fitting the pressure-volume data using the Murnaghan equation of state.

Key words: $SrMnO_3$, high-pressure, structure, phase transition, X-ray diffraction

PACS: 91.60.Gf, 91.60.Fe, 91.60.Hg **DOI:** 10.1088/1674-1137/35/5/022

1 Introduction

Hexagonal ABX_3 perovskites are less common than cubic ones, and are typically formed when the A cations are too large to be accommodated in the BX_6 framework. It is well known that alkali-earth manganese oxides are typical compounds, which change from the ideal $Pm3m$ perovskite-structure to a more distorted structure according to the radius of the A cation [1]. The ionic radius increases from r_{Ca2+}=1.34 Å (radius for 12-coordination) to r_{Ba2+}=1.61 Å, with r_{Sr2+}=1.44 Å in the middle [2]. Correspondingly, the $CaMnO_3$ perovskite forms an orthorhombic derivative of the ideal cubic structure, while $BaMnO_3$ crystallizes in a hexagonal structure in which all MnO_6 octahedra share faces along the c axis (2H-type).

$SrMnO_3$ is a rare example that has both cubic and hexagonal polymorphs, and a 4H type structure with alternating face-sharing and corner-sharing MnO_6 octahedra along the c axis. Due to its structural particularity, $SrMnO_3$ has been widely studied for more than forty years, including its electrical conductivity [3, 4], thermal conductivity [5], magnetic property [1, 6, 7], and structural characteristics under different conditions [8–10]. Up to now, only a few high-pressure experiments of hexagonal perovskites have been found in the literature. The earliest in-situ high-pressure energy dispersive X-ray diffraction (EDXD) experiment was done by Wu, who observed no phase transition of $SrMnO_3$ up to 20.6 GPa [11]. Søndenå et al. [1] gave the isothermal bulk modulus of $SrMnO_3$, subsequently. Recent Raman experimental studies have shown that one analogue $Ho_{0.8}Dy_{0.2}MnO_3$ is transformed from hexagonal $P6_3cm$ to an orthorhombic structure near 9.8 GPa [12]. Therefore, a similar high-pressure behavior of $SrMnO_3$ has been speculated. However, previous experiments of $SrMnO_3$ were done using EDXD molde with lower energy and poor resolution, which makes it hard to judge its phase transition. In order to understand its structural stability better, here we report the high-pressure behavior of $SrMnO_3$ up to 28.6 GPa in detail.

Received 13 July 2010, Revised 27 August 2010
* Supported by National Natural Science Foundation of China (40972029)
1) Corresponding author, E-mail: sqin@pku.edu.cn

2 Experiments

The $SrMnO_3$ sample used in this study was synthesized using the standard solid state method. The reagents $SrCO_3$ and MnO_2 (Chempur, 99.9%) were dried for 5 hours at 500 degrees centigrade. Mixtures of stoichiometric amounts were heated form 500 to 1000 degrees centigrade at a rate of 30 degrees centigrade per hour, then cooled down to room temperature in a furnace slowly. After periodic regrinding in an agate mortar, the samples were fired from 1000 to 1400 degrees centigrade in air. After that, the samples were kept at 1400 degrees centigrade for more than 23 hours, and then cooled rapidly to room temperature in air. Quantitative chemical analyses were obtained using a JEOL JXA-8100 electron microprobe (EMP) at the Key Laboratory of Orogenic Belts and Crustal Evolution of MOE, Peking University. The system was operated using a defocused electron beam (ϕ1 μm) at an accelerating voltage of 15 kV and with a beam current of 10 nA. A range of standard minerals from SPI was used for standardization and all data were reduced using the PHZ correction routine. The resulting chemical formula represents an average of 3 analyses and was calculated on a 3-oxygen basis (Table 1).

Table 1. Chemical composition of $SrMnO_3$. $\bar{x}$: average values over three EMP data.

	MnO_2	SrO	CaO	Mn (wt.%)	Sr (wt.%)	Ca (wt.%)	O (wt.%)	Mn/mol	Sr/mol	Ca/mol	O/mol
1	45.77	53.68	0.062	28.92	45.39	0.04	25.15	1.000	0.988	0.002	3
2	45.14	54.90	0.049	28.52	46.42	0.04	25.11	0.993	1.013	0.002	3
3	45.36	54.09	0.067	28.66	45.74	0.05	25.07	0.999	1.000	0.002	3
$\bar{x}$	45.42	54.22	0.059	28.70	45.85	0.04	25.11	0.999	1.000	0.002	3

The high-pressure angular dispersive X-ray diffraction (ADXD) measurement was performed at Beam Line 13A, KEK, in Japan, with a 400 μm culet Mao-Bell Diamond Anvil Cell (DAC) and an imaging plate detector. The X-ray beam was focused to a 50 μm×50 μm dimension. Monochromatic synchrotron radiation at λ=0.4263 Å was used for data collection with 2θ ranging between 5° and 22°. Twenty runs up to 28.6 GPa were carried out. A typical exposure time of about 7 min was employed for a diffraction pattern at high pressure.

16:4:1 methanol-ethanol-water mixture was used as the pressure medium in DAC, with T301 stainless steel as the sealing gasket. The $SrMnO_3$ samples were ground into powder and loaded together with a ruby chip into a 200 μm hole, which was drilled on a gasket and pressurized to 50 μm thick. The pressure was measured by the shift of the R1 photoluminescence line of ruby [13].

3 Results and discussion

Two-dimensional ring patterns were processed using the program WINPIP in order to yield the intensity versus 2θ plots. The phase analysis was performed by fitting the ADXD profile with the Rietveld method using the GSAS software [14]. Refined parameters include histogram scale factors, background coefficients, zero point shift, lattice parameters, atomic positions, profile parameters, and linewidths. Cell parameters a=5.4426(8) Å and c=9.0793(16) Å of $SrMnO_3$ under ambient conditions were obtained, which are in good agreement with other experimental values [6, 8, 15, 16].

The selected patterns of different pressures up to 28.6 GPa are illustrated in Fig. 1. All of these diffraction lines have been normalized and eliminated the backgrounds. More than 20 diffraction peaks were observed and indexed at normal atmospheric pressure, with several peaks indexed as the reaction residues. With an increase in pressure, all of these peaks shift toward higher degrees. Due to the lower initial intensity, couples of peaks seem to merge into one at 28.6 GPa, such as 202 and 104 near 12°, 212 and 204 around 15°. In order to figure them out, we plotted the analysis result of the representative 202 and 104

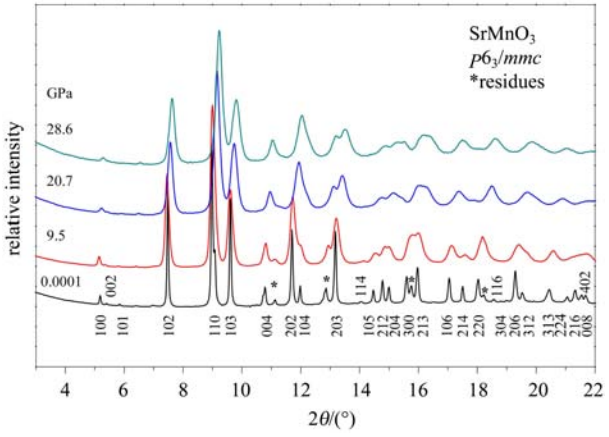

Fig. 1. Selected ADXD patterns of $SrMnO_3$ at different pressures.

peaks in Fig. 2. It can be seen that the calculated pattern is in better agreement with the observed pattern when two peaks are used, which means that the weak diffraction line has only been covered by the higher one. Similar fitting results were also obtained in other peaks up to 28.6 GPa, which indicates that the structure of $SrMnO_3$ is unchanged. According to the fitting result, the $P6_3/mmc$ structure model was used to refine the pattern under 28.6 GPa and satisfactory results were obtained (Fig. 3).

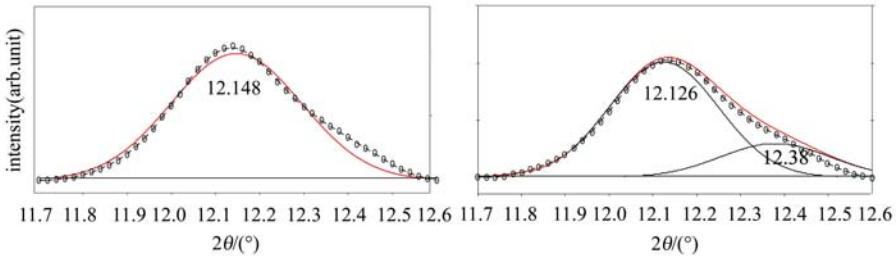

Fig. 2. The observed ADXD pattern (ellipses and dash lines) of $SrMnO_3$ between 11.7° and 12.6° compared with the calculated pattern (solid lines) at 28.6 GPa (the right pattern fitted with two peaks was more matchable than the left one, which was calculated with one peak).

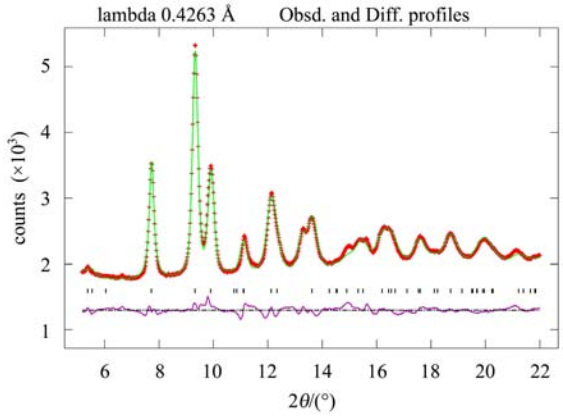

Fig. 3. The observed (shown as crosses), calculated (solid line on the crosses) and difference (solid line below the ticks) plots from the structural refinement of $SrMnO_3$ ($P6_3/mmc$) against the ADXD data collected at 28.6 GPa. Tick marks indicate the calculated positions of peaks.

Values of cell parameters as a function of pressure are listed in Table 2. The relative compression of unit cell parameters is plotted in Fig. 4. As shown in this figure, it can be seen that the a axis is more compressible. The compression ratios are β_a=1.11×10^{-3} GPa^{-1} and β_c=0.85×10^{-3} GPa^{-1}, with β_a: β_c=1: 0.77. According to the GSAS refinement, the average bond distance of Mn-O in MnO_6 polyhedra is Mn-O1=1.9246 Å and Mn-O2=1.8460 Å originally. When the pressure is up to 28.6 GPa, the bond distances change to 1.8750 Å and 1.6394 Å, respectively, which suggests that the torsion of MnO_6 octahedra is increased. These phenomena can be explained by their high-pressure crystal structure (Fig. 5). It is well known that the d-spacing in a unit cell decreases with increasing pressure. Therefore, the Mn-Mn distance gets shorter at higher pressure. According to Pauling's rules, the repulsive force will play a dominant role when the Mn-Mn distance gets short enough. Correspondingly, the Mn-Mn distance shortens with more and more difficulty because of the stronger repulsive force. While the pressure continues to be loaded, the MnO_6 octahedra will be distorted more obviously along their corner-sharing directions, which are almost parallel to the a axis. This may be the potential reason for the higher compressibility of the a axis.

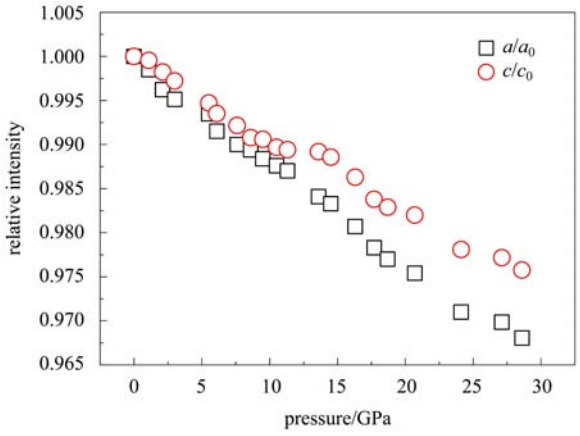

Fig. 4. Relative compression of $SrMnO_3$, showing the variation in relative axial ratios as a function of pressure.

The Murnaghan equation of state (EOS) was used to fit the pressure-volume (P-V) data, where V_0, K_{298} and K_0' are the volume per unit cell, the bulk modulus and its pressure derivative at zero pressure, respectively. The isothermal bulk modulus K_{298}=266(4)

Table 2. Cell parameters of $SrMnO_3$ as a function of pressure.

P/GPa	a/Å	c/Å	V/Å^3	R_p(%)	wR_p(%)
0.0001	5.4426(8)	9.0793(16)	232.9(1)	2.95	5.50
1.1	5.4345(13)	9.0754(22)	232.1(1)	4.34	7.07
2.1	5.4221(16)	9.0634(28)	230.8(2)	3.83	5.56
3.0	5.4161(20)	9.0542(36)	230.0(2)	3.99	5.71
5.5	5.4072(21)	9.0314(36)	228.7(2)	2.98	4.56
6.1	5.3964(20)	9.0207(34)	227.5(2)	2.89	4.33
7.6	5.3884(20)	9.0083(35)	226.5(2)	3.18	4.79
8.6	5.3848(20)	8.9956(36)	225.9(2)	3.47	5.07
9.5	5.3797(17)	8.9942(31)	225.4(2)	3.06	4.55
10.5	5.3751(16)	8.9860(30)	224.8(2)	3.06	4.51
11.3	5.3720(16)	8.9832(28)	224.5(2)	2.99	4.45
13.6	5.3560(19)	8.9812(34)	223.1(2)	2.72	3.99
14.5	5.3516(51)	8.9755(83)	222.6(5)	2.63	3.78
16.3	5.3373(20)	8.9547(36)	220.9(2)	2.24	3.90
17.7	5.3245(20)	8.9322(35)	219.3(2)	2.16	3.17
18.7	5.3174(23)	8.9237(41)	218.5(2)	2.11	3.07
20.7	5.3087(27)	8.9157(48)	217.6(3)	2.24	3.22
24.1	5.2846(27)	8.8801(47)	214.8(3)	1.87	2.83
27.1	5.2785(27)	8.8721(48)	214.1(3)	1.88	2.78
28.6	5.2688(31)	8.8592(56)	212.8(3)	1.87	2.78

Note: the numbers in parentheses are the estimated standard deviation in units of the last digit(s). R_p and wR_p are the expected profile R-factor and the weighted profile R-factor in the Rietveld refinements.

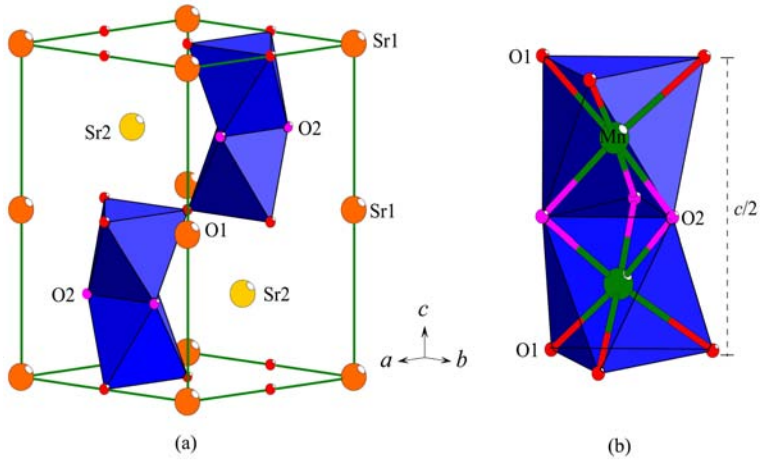

Fig. 5. Schematic structure of $SrMnO_3$ (a) and MnO_6 octahedra (b) at 28.6 GPa.

GPa and $V_0 = 232.9(1)$Å^3 are obtained (Fig. 6) Here, we fixed K'=4, which is a commonly accepted value for silicates and oxides [17].

In the literature, only Søndenå et al. [1] studied the P-V EOS of $SrMnO_3$ and gave K_{298}=126 GPa (calculated result) and 136 GPa (experimental result), which are lower than the value reported here. The K_{298}=177 GPa obtained by Wu [11] is also lower than our data. After comprehensive comparison with previous studies, it is assumed that the difference in the isothermal bulk modulus might be triggered by the following factors. On the one hand, the cell parameters that we calculated under ambient conditions are smaller than others, especially the cell parameters a=5.489 Å and c=9.114 Å obtained by Søndenå [1]. On the other hand, the pressure-transmitting medium and pressure gauge used in our experiments are different from those used by Søndenå (nitrogen as pressure-transmitting medium) [1] and Wu (Pt powder as pressure gauge) [11]. Furthermore, the pressure we achieved may be higher than the actual pressure due to the pressure gradient in the sample chamber, which was caused by the unsatisfactory position of the ruby chip. Thus, all of these factors might cause the difference between the EOS parameters in this study and the reported ones in the

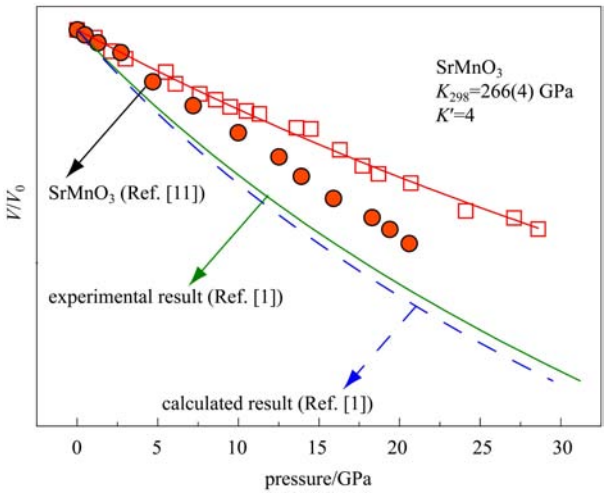

Fig. 6. Pressure dependence of unit cell volume of $SrMnO_3$.

literature [1, 11].

In future experiments, more attention should be paid to ensure the hydrostatic pressure environment and to reduce the pressure gradient caused by the position of the pressure gauge. Additionally, first-principles calculations will be used to study the structure stability and other physical properties of $SrMnO_3$ under high pressure conditions.

4 Conclusions

The in-situ high-pressure structures of $SrMnO_3$ ($P6_3/mmc$) have been investigated using ADXD and DAC techniques under pressure up to 28.6 GPa. The experimental results confirm that $SrMnO_3$ has no phase transition in this pressure range. By linear fitting, the axial compression coefficients of $SrMnO_3$ are obtained with β_a=1.11×10^{-3} GPa^{-1}, β_c= 0.85×10^{-3} GPa^{-1}, respectively. The reason why the a axis is more compressible is explained by the high-pressure structure behavior of $SrMnO_3$. The pressure dependence of cell volume is fitted to the Murnaghan EOS, yielding a room-temperature isothermal bulk modulus K_{298}=266(4) GPa.

References

1 Søndenå R, Ravindran P, Stølen S. Physical Review B, 2006, **74**: 144102/1
2 Shannon R D. Acta Crystallographica A, 1976, **32**: 751
3 Lee K J, Iguchi E. Journal of Solid State Chemistry, 1995, **114**: 242
4 Hashimoto S, Iwahara H. Journal of Electroceramics, 2000, **4**: 225
5 Chmaissem O, Dabrowski B, Kolesnik S et al. Physical Review B, 2001, **64**: 134412/1
6 Battle P D, Gibb T C, Jones C W. Journal of Solid State Chemistry, 1988, **74**: 60
7 Töpfer J, Pippardt U, Voigt I et al. Solid States Sciences, 2004, **6**: 647
8 Negas T, Roth R S. Journal of Solid State Chemistry, 1970, **1**: 409
9 Mori T, Kamegashira N. Journal of Alloys and Compounds, 2000, **313**: L1
10 Sacchetti A, Baldini M, Postorino P et al. Journal of Raman Spectroscopy, 2006, **37**: 591
11 WU X. PhD thesis in Chinese Academy of Sciences. 2005, p.74
12 FENG S M, WANG L J, ZHU J L. Journal of Applied Physics, 2008, **103**: 026102/1
13 MAO H K, XU J, Bell P M. Journal of Geophysical Research-Solid Earth, 1986, **91**: 4673
14 Larson A C, Von Dreele R B. GSAS: General Structural Analysis System, LANSCE, Los Alamos National Laboratory, Los Alamos, NM, The Regents of the University of California, 1994
15 Chamberland B L, Sleight A W, Weiher J F. Journal of Solid State Chemistry, 1970, **1**: 506
16 Kuroda K, Ishizawa N, Mizutani N et al. Journal of Solid State Chemistry, 1981, **38**: 297
17 Holland T J B, Redfern S A T, Pawley A R. American Mineralogist, 1996, **81**: 341